Adaptive Neuro Fuzzy Inference System Based Decoupled Control for Neutral Point Clamped Multi Level Inverter Fed Induction Motor Drive

Giribabu Dyanamina and Sanjay Kumar Kakodia*

(Department of Electrical Engineering, Maulana Azad National Institute of Technology, Bhopal, M.P 462003, India)

Abstract: The presence of an integrator in a reference model of a rotor flux-based model reference adaptive system (RF-MRAS) and non-linearity of the inverter in the output voltage degrade the speed response of the sensorless operation of the electric drive system in terms of DC drift, initial value issues, and inaccurate voltage acquisition. To improve the speed response, a compensating voltage component is supplemented by an amending integrator. The compensating voltage is a coalition of drift and offset voltages, and reduces DC drift and initial value issues. During low-speed operation, inaccurate voltage acquisition distorts the stator voltage critically, and it becomes considerable when the stator voltage of the machine is low. Implementing a three-level neutral point clamped inverter in speed-sensorless decoupled control of an induction motor improves the performance of the drive with superior quality of inverter output voltage. Further, the performance of the induction motor drive is improved by replacing the proportional-integral (PI) controller in the adaption mechanism of RF-MRAS with an adaptive neuro-fuzzy inference system (ANFIS) controller. A prototype model of the three-level neutral point clamped inverter (3L-NPC)-fed induction motor drive is fabricated in a laboratory, and its performance for a RF-MRAS, modified RFMRAS, and modified RFMRAS using ANFIS are compared using different benchmark tests.

Keywords: Induction motor drive, vector control, neutral point clamped inverter, model reference adaptive system, ANFIS

1 Introduction

Controlling the induction motor (IM) drives is necessary to meet the speed and torque demands of industries. This is because it significantly affects energy saving in variable frequency drive (VFD) systems. Initially, DC motors were used for industrial applications because of their simple control. The DC motor drives naturally provide decoupled torque and flux control. However, these machines have a commutator, which corrodes, sparks, and requires frequent maintenance. AC motor drives are alternatives for DC motor drives with advancement in power semiconductor and digital signal processing technologies [1-2]. However, the control of IM is difficult because it is a singly excited machine. Its torque and flux characteristics are interdependent and obligate complex non-linear models.

Converter control plays a crucial role in VFD. The converter draws power from a constant power source. For the VFD operation, rectification and inversion are simultaneously required to change the magnitude of the voltage and frequency. The rectifier changes the voltage while the inverter changes the frequency of the operation [3]. Conventional two level inverter is used for speed control of IM. In this case, switching of the lower and upper switches in the half-bridge inverter generates a phase voltage with positive and negative magnitudes ($+0.5V_{dc}$, $-0.5V_{dc}$). If the inverter power level and fundamental voltage level increase to a high value, the switches are connected in a series configuration to achieve the rated capacity of the switch. In the series configuration, the normal operation is simple. However, dynamic voltage sharing is difficult; thus, a multilevel or neutral point clamped (NPC) inverter is introduced to address this

Manuscript received July 23, 2020; revised October 3, 2020; accepted October 29, 2020. Date of publication June 30, 2021; date of current version June 3, 2021.

* Corresponding Author, E-mail: dgiribabu208@gmail.com

Digital Object Identifier: 10.23919/CJEE.2021.000017

issue. These inverters are well-known for excellent performance in terms of less stress across power electronics devices, smoother voltage response, and digital implementation [4]. The output voltage level increases the control complexity. If the number of output levels is n, then (n–1) DC link capacitors are required; hence, making the system more costly and bulky. The neutral point is created by splitting the DC bus voltage.

Speed control using scalar control of the IM drive yields a decent steady-state performance; however, its dynamic response is slow. In modern high-performance AC drives for speed control, the vector control (VC) scheme is employed because of better transient and steady-state response at all speed ranges. The speed response of the VC method is dependent on the machine parameters [5-6]. The VC method is also known as field-oriented control (FOC), and is classified into two categories: Indirect-FOC (IFOC) and Direct-FOC (DFOC) [7]. The closed-loop speed control operation of a drive requires a speed encoder/position sensor, which deteriorates the speed response of the drive system, and its installation escalates hardware difficulty, cost, added size to the motor, and limits drive operation in a hostile environment [8]. To avoid frequent maintenance of the encoder and to improve the reliability of the drive, speed estimation techniques are used. In the literature, different techniques have been proposed, such as high-frequency injection, rotor slot bar information, Kalman filter, sliding mode observer (SMO), model reference adaptive system **(**MRAS), Luenberger observer, and AI-based techniques [9-11].

A contemporary method known as direct torque control (DTC) was introduced in the early 1980s. This method uses hysteresis controllers and utilizes the ideal switching combination of an inverter for better dynamic response at varying load torques [12]. However, its performance is poor at low speeds, because it is difficult to control the flux and torque at low speeds [13-15]. In Ref. [16], the limitation of DTC is rectified using predictive torque control (PTC) without start-up issues. Improved PTC has been proposed to enhance the selection of the weighting factor. However, this method has a poor dynamic response near zero speed operations [17]. The vector control scheme was implemented using a high-frequency signal injection method, and it produces a high-frequency rotating magnetic field (RMF) as well as interacting with the main RMF. The zero-sequence voltage is demodulated using a suitable technique. However, at low speed region, the third harmonics are insufficient to measure. It uses extra circuitry for the injection of the signal and reduces the reliability of the drive [18-19]. These techniques require machine-parameter knowledge to estimate the rotor speed. A slight variation in machine parameters owing to temperature change and inaccurate measurement of machine parameters causes inaccurate speed estimation, which affects the IM drive performance. The MRAS technique is well explained in the literature and is preferable owing to its simple structure, direct substantial explanation, and amnesty to machine parameter variation [20]. The MRAS speed estimators are classified according to error signal minimization as rotor flux [21]; stator current [22] measured from reference and adaptive models; active and reactive power [23]; or back electromagnetic force (EMF). Reactive-power-based MRAS yields remarkable performance at low speeds, and is independent of the stator resistance variation. However, this scheme is unstable in regenerative mode. The model reference adaptive principle (MRAP) reported in Ref. [24] is based on the machine algebraic model instead of a dynamic model. MRAP improves the IM drive performance in the field weakening region. A novel MRAS technique using steady-state and instantaneous voltage and current vectors has been proposed [20]. The reference model uses the $\boldsymbol{V}^{*}\times\boldsymbol{i}$ quantity, while the adjustable model uses the stator steady-state oriented quantity.

Speed estimation using back-EMF has satisfactory low-speed operation, but experiences noise and stator parameter sensitivity at high-speed operations. The speed response at low speed is improved by reactive power based MRAS, but it has rotor parameter sensitivity. The effect of the integrator on the drive performance and its minimization methods are reported in the Refs. [22-25]. The DC drift and initial problem in the voltage model of the RF-MRAS is improved by modification in the integrator. Recent research on speed sensorless techniques suggests new

approaches to minimize the integrator issues. The adaptive model of the MRAS is modified for an accurate estimation of the rotor speed based on the stator current. This technique experiences a stability problem because the estimated speed depends on the stator current. In place of the integrator, a low pass filter (LPF), which has a lower cut-off frequency, has been employed. This LPF degrades the observer dynamic performance below the cut-off frequency, and a programmable cascaded LPF with less time constant replaces the LPF to limit the DC offset decay time effect [26]. Raute et al. [27-28] suggested an observer for speed sensorless control to improve DC drift, the compensation of dead time, and offset voltage of the non-linear integrator model using harmonics; however, harmonic extraction is critical as it depends on the rotor bar slot position.

The PI controller in the adaptive scheme alters the speed response at low-speed operation of the drive. Furthermore, the response is improved by the AI instead of the conventional PI controller, for instance, the neural network controller (NNC) and fuzzy logic controller (FLC) or a combination of both Refs. [29-30]. The RF-MRAS speed technique has more torque ripples. The current drawn by the motor is distorted [31]. In the estimation of the rotor speed, SMO makes the system more stable based on the Lyapunov theory [32]. The FLC is used for nonlinear optimization to minimize the speed tuning error. More mathematical computation is required for the combination of FLC and SMO. An artificial neural network (ANN) controller is presented in Refs. [33-34] to estimate rotor speed. The neural network (NN) is used instead of the rotor flux observer in the current model to solve the stability problem in the low-speed regenerative operation of the IM drive. The ANN-based scheme has better performance at low-speed operation; however, it experiences stability issues in the speed-torque region when the drive is in regenerative mode. To avoid the pure integrator, the measured current is utilized in the voltage model of the MRAS observer. To improve the dynamic and steady-state drive response, the adaptive neuro-fuzzy inference system (ANFIS) controller with modified RF-MRAS is implemented in this study. The ANFIS uses the advantages of FLC and NNC [35]. This technique has remarkable performance in comparison to other techniques, and is immune to drive parameter variation.

Fig. 1a illustrates the proposed control scheme block diagram, and Fig. 1b illustrates the one-leg switch connection configuration of neutral point clamped inverter. The paper is organized as follows. In Section 2, sensorless FOC control of NPC-fed IM drive is presented, in which the conventional RF-MRAS, modified RF-MRAS, and ANFIS controller are based on a modified RF-MRAS speed estimator. In Section 3, the development of a prototype model of the proposed ANFIS-based speed estimator using the dSPACE DS-1104 R&D board controller is elaborated. Similarly, in Section 4, the proposed drive performance at different benchmark tests, such as no-load, load rejection capability in forward and reverse motoring mode, and rapid change in speed and load torque, is presented. In Section 5, the proposed ANFIS controller scheme-based drive system performance is discussed, and conclusions are drawn.

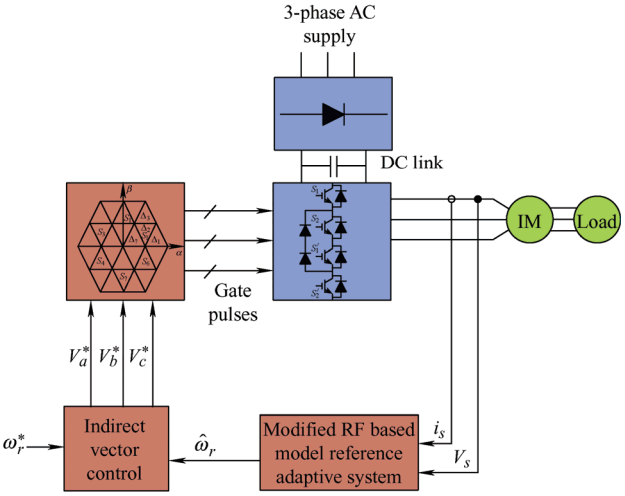

(a) Indirect vector control of the IM drive based on ANFIS

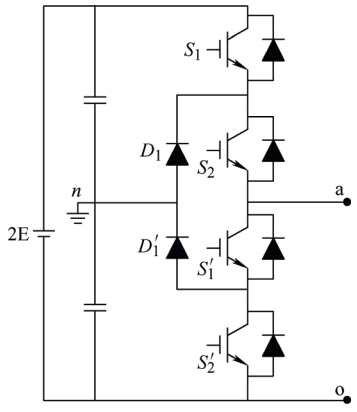

(b) One leg of the NPC inverter

Fig. 1 Diagrammatical representation of indirect vector control

2 Sensorless field oriented control of NPC-fed IM drive

2.1 Conventional RF-MRAS

The RF-MRAS speed estimator has two models: reference and current models. The reference model, which is autonomous with the estimated quantity (rotor speed), is called the voltage model. The current model, which depends on an estimated quantity, is called an adaptive model. The rotor speed is estimated using the error produced by comparing both models. The stator voltage equations of IM are used to derive the voltage model(VM). The adaptive model is derived from the IM rotor voltage equation. The block diagram of conventional RF-MRAS presented in Fig. 2 has a simple design, and its performance is satisfactory over a wide speed range; however, it depends on the machine parameter. This variation affects the system performance. The current and voltage models as well as rotor speed are provided by Eqs. (1)-(6).

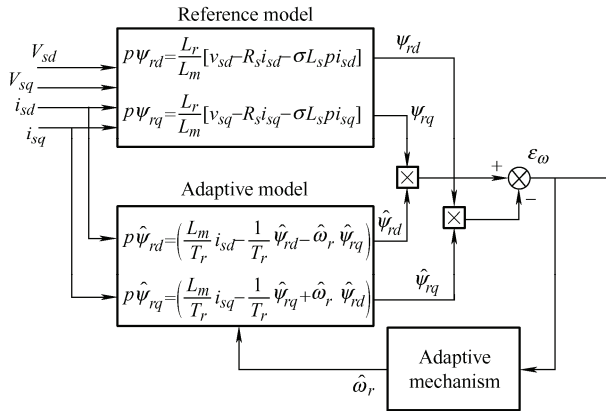

Fig. 2 Structure of the conventional RF-MRAS

$$p\psi_{rq}=\frac{L_r}{L_m}\left(v_{sq}-R_s i_{sq}-\sigma L_s p i_{sq}\right) \tag{1}$$

$$p\psi_{rd}=\frac{L_r}{L_m}\left(v_{sd}-R_s i_{sd}-\sigma L_s p i_{sd}\right) \tag{2}$$

$$p\hat{\psi}_{rq}=\left(\frac{L_m}{T_r}i_{sq}-\frac{1}{T_r}\hat{\psi}_{rq}+\hat{\omega}_r\hat{\psi}_{rd}\right) \tag{3}$$

$$p\hat{\psi}_{rd}=\left(\frac{L_m}{T_r}i_{sd}-\frac{1}{T_r}\hat{\psi}_{rd}-\hat{\omega}_r\hat{\psi}_{rq}\right) \tag{4}$$

$$\varepsilon_\omega=\psi_{rq}\hat{\psi}_{rd}-\psi_{rd}\hat{\psi}_{rq} \tag{5}$$

$$\hat{\omega}_r=\left(K_{p\omega}+\frac{K_{i\omega}}{p}\right)\varepsilon_\omega \tag{6}$$

where ψ_{rd},ψ_{rq} are the rotor *d-q* axis flux components and $\hat{\psi}_{rd},\hat{\psi}_{rq}$ are the estimated flux components of the rotor *d-q* axis of the IM drives. R_s is the stator winding resistance, L_s, L_r and L_m are the self-inductance of the stator, rotor, and mutual inductance of the IM, respectively. σ, p are the leakage coefficient, pole pair, respectively. v_{sd}, v_{sq} are the stator *d-q* axis voltage components. i_{sd}, i_{sq} are the rotor *d-q* axis current components. T_r, ε_ω are the rotor time constant and error vector, respectively. $\hat{\omega}_r$ is the estimated rotor speed and $K_{p\omega}$, $K_{i\omega}$ are the parameters of the PI controller in the IM drive.

2.2 Modified voltage model for conventional RF-MRAS

The conventional RF-MRAS has poor speed response, particularly at low speed ranges owing to limitations during its practical implementation. The causes of the exertion are the existence of the integrator in its structure, non-linearity of the inverter, and acquisition of voltage. The issue of DC drift in the integrator limits the practical implementation; the integrator introduces a large error in the estimation of flux position, and this flux angle has phase modulation at the fundamental frequency during the control of current and voltage vectors. The dead time of the switches causes inaccurate information of the estimated flux, which mismatches the rotor flux component of the adaptive and reference models. The actual rotor flux component is different from the estimated value; thus, affecting the estimated rotor speed.

Fig. 3 illustrates the block diagram of the modified RF-MRAS. In this case, the VM of RF-MRAS is changed to reduce the drift problem, and the PI controller in the adaptive mechanism is replaced with the ANFIS controller, which enhances the low-speed performance. The modification is explained by the addition of a compensating voltage term to its reference model component. This voltage term is derived from the non-linear integration model, with a change in the set speed at different values. The compensating voltage term enhances the addition of the component to the estimated rotor flux component, thus diminishing the speed tuning error. The actual machine model of RF-MRAS is adapted to equalize

the voltage and current models of the rotor flux components.

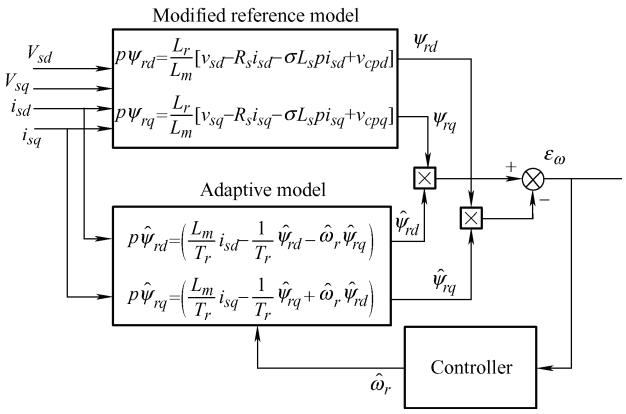

Fig. 3 Block diagram of modified RF-MRAS

Fig. 4 illustrates the internal structure of the modified RF-MRAS. The drift voltage and offset voltage are required to calculate the compensating voltage component, where the offset voltage is an indelicate term that is retrieved by integrating the induced voltage; thus, forms a signal represented as ψ_{rd1} or ψ_{rq1} for rotor flux *d*-*q* axis components. DC offset constituent in the back EMF is eliminated from the fundamental value of the induced voltage and is restricted to rotor flux reference value ψ_r^*. The final offset voltage is the output of the fundamental flux constituent and initial machine flux value. Furthermore, based on this modification of reference model, computation of offset voltage from the fundamental flux is simple compared to other techniques. The calculation of the compensating voltage term is explained as

$$\psi_{rq} = \frac{L_r}{L_m}\int\left(v_{sq} - R_s i_{sq} - P\sigma L_s i_{sq} + v_{cpq}\right)\mathrm{d}t \tag{7}$$

$$\psi_{rd} = \frac{L_r}{L_m}\int\left(v_{sd} - R_s i_{sd} - P\sigma L_s i_{sq} + v_{cpd}\right)\mathrm{d}t \tag{8}$$

$$v_{cpd} = v_{driftd} + v_{offsetd} \tag{9}$$

$$v_{cpq} = v_{driftq} + v_{offsetq} \tag{10}$$

d-axis offsets voltage is calculated with the induced voltage v_{d1} and expressed as

$$v_{d1} = v_{sd} - R_s i_{sd} - P\sigma L_s i_{sd} \tag{11}$$

$$\psi_{rd1} = \int v_{d1}\mathrm{d}t \tag{12}$$

$$v_{offsetsd} = \psi_{rd1}.\psi_0 \tag{13}$$

The reference rotor flux and rotor flux *d*-axis

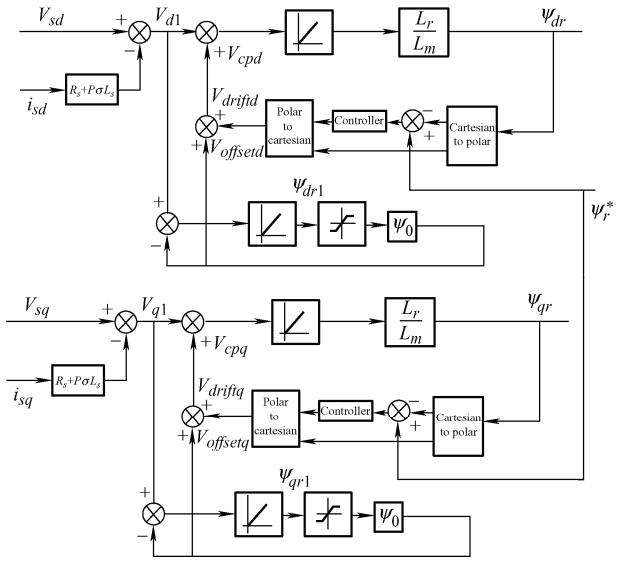

Fig. 4 Internal structure of the modified RF-MRAS

constituent are used in the computation of the *d*-axis drift voltage, and by changing the polar form to Cartesian, the final output becomes

$$v_{driftd(k)} = \psi^*_{r(k)} - \psi_{dr(k)} \tag{14}$$

$$\Delta v_{driftd(k)} = v_{driftd(k)} - v_{driftd(k-1)} \tag{15}$$

The *q*-axis drift and offset voltage are computed in the same manner. The low-speed performance even at zero-speed operation is improved in the modified RF-MRAS as compared to conventional speed estimation because the compensating voltage term is added to the rotor flux; thus, the speed tuning error is improved in the presence of leakage reactance factor of the rotor, whereas in other methods, the term rotor leakage reactance factor is not considered in the flux estimation.

2.3 ANFIS based modified RF-MRAS

The low-speed operation of the IM drives is improved by using ANFIS instead of the conventional PI controller. This is because ANFIS is more robust to the drive-parameter variations. The system transient response is further improved by avoiding the use of filters. With the ANFIS-based controller, speed estimation is faster because the delay in the conventional PI controller below the cut-off frequency is eliminated. The ANFIS is an intelligent hybrid system based on the NN and fuzzy logic principle. The ANFIS is considered as an ideal approximation tool. The ANFIS architecture shown in Fig. 5 is similar to the Tsukamoto fuzzy inference

system (FIS). For simplicity, the modified RF-MRAS with ANFIS structure has two inputs (x_1 and x_2) with one output function (R). Suppose that the rule base consists of two fuzzy inputs, then the "if-then" rules of the Takagi and Sugeno types are used. The ANFIS uses a first-order Sugeno-style FIS, which is presented in Refs. [27-28], the rules are described as follows.

Rule 1: If x_1 is A_1 and y is B_1 then $f=m_1x+n_1y+c$;

Rule 2: If x_1 is A_1 and y is B_1 then $f=m_2x+n_2y+c$

The ANFIS presented consists of five layers and are illustrated as follows.

Layer 1: In the ANFIS model, the first layer is represented as layer 1, where every node is denoted as a square. This layer is also called a fuzzification layer. Every input in the layer contains three membership functions (MF). These are used to minimize the computational burden. The error value is used to adjust the parameter value and produce the linguistic value of the MFs. The parameter in this layer is called a precondition parameter.

Layer 2: The output of layer 1 is an input signal for layer 2. The function of this layer is to produce the incoming signal and pass this to the next layer, i.e., layer 3. It is represented as a circle in the ANFIS diagram and denoted as pi (π). The firing strength of each rule is characterized by every node, and is written as

$$w_i=\mu_{Ai}(x)\times\mu_{Bi}(y)$$

Layer 3: The third layer in the ANFIS model is drawn as a circle for every node and is denoted as N. In this layer, the normalized firing strength of each rule is calculated, which is written as

$$\overline{w}_i=\frac{w_i}{w_1+w_2}\quad \text{for } i=1,2$$

Layer 4: Each node in layer 4 is a square node and is represented as a node function. The parameter of this layer is known as a consequent parameter, and is written as

$$o_i^4=\overline{w}_i f_i=\overline{w}_i(m_ix+n_iy+c)$$

where $\overline{w}_i$ denotes the output of layer 3 and the terms $\{m_i,n_i,c\}$ are parameter set.

Layer 5: This layer contains a single node represented as a circle in the ANFIS model and is denoted as Σ. This single node is an output of the summation of all incoming signals.

$$o_i^5=\text{overall output}=R=\sum_i\overline{w}_i f_i=\frac{\sum_i w_i f_i}{\sum_i w_i}$$

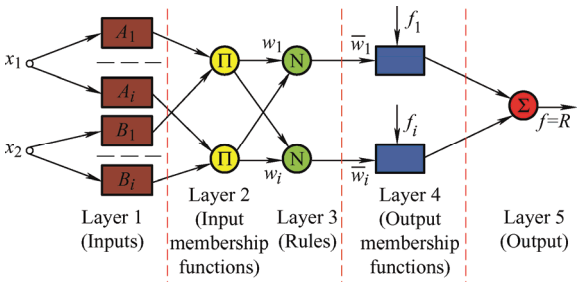

Fig. 5 Structure of the ANFIS controller

The ANFIS training is performed offline with ANFIS-editor in Matlab software using trained data and is processed in the simulation by the gradient descent method and least square estimation (LSE). The training dataset for ANFIS is obtained from the workspace with the input-output data pattern. The performance of the sensorless controlled IM drive is validated under various operating conditions, and this data is used for experimentation. The ANFIS-based speed estimator, modified RF-MRAS, and conventional RF-MRAS speed estimator performance are compared using different benchmark tests.

3 Practical implementation of proposed model

The speed sensorless vector control performance of the IM drive is validated with a dSPACE DS 1104 R&D laboratory prototype. The machine parameters used for prototype development are listed in Tab. 1. A pictorial view of the experimental setup of the sensorless speed controller of the IM drive is presented in Fig. 6. The prototype model has a voltage source inverter (VSI), three-phase IM, and sensors (voltage, current, and speed sensors). The intelligent power module (IPM) (PEC16DSM03) VSI is used to supply power to the IM drive system. It consists of a three-phase diode bridge converter for converting supply from the AC to DC supply and a full-bridge VSI using an insulated gate bipolar transistor (IGBT) to convert voltage from DC to AC supply. The Hall effect based-current sensor measures the motor line currents; the DC link voltage is measured by an LEM LV25P-type voltage sensor, and upper gate pulses are utilized to minimize the effect of dead time during practical implementation.

Tab. 1 Machine parameter values and ratings

Parameter	Value
Nameplate capacity	1 HP
Stator resistance/Ω	10.124
Rotor resistance/Ω	8.973 8
Stator inductance/H	0.533 9
Mutual inductance/H	0.490 5
Rotor inductance/H	0.523 9
Inertia constant/(kg • m^2)	0.001 9
Synchronous speed/(r/min)	1 500
Pole pairs	2
Rated supply frequency/Hz	50
Friction coefficient/(N • m • s)	0.028 5
Rated voltage/V	415
Rated current/A	12
Phases	3

The RF-MRAS voltage and current model equations are implemented using sensor circuitry. It is important to measure the rotor speed of the IM using the sensorless technique for verification of the estimated speed. Therefore, HEDS-5645 incremental optical encoder is used; it consists of 512 encoder lines per revolution. VSI driving pulses are generated with SVPWM using a digital controller dSPACE, DS1104 R&D controller board. This DS1104 has a PPC6603e core processor operating at 250 MHz and Texas instrument TMS320F240 DSP 20 MHz clock frequency working as the slave DSP subsystem. The inverter switching frequency for SVPWM implementation is 5 kHz with a device dead time set as 1 μs, and the sample time of the speed observer along with the control loop is set as 60 ms.

Fig. 6 Pictorial view of the experimental setup for sensorless speed controller

4 Experimental results

For the experimental validation of the prototype, the stator voltage was taken as the reference model. The voltage sensor shows the voltage measurement inaccuracy. The low-speed operation of the drive is affected by inaccurate measurement when the drive is operated in the low-speed region, and the rotor flux error becomes influential value. By controlling the DC link voltage or using the switching pulse of the upper and lower switch pair, we can reduce the rotor flux inaccuracy. The ANFIS-based speed estimation technique is compared with both conventional and modified RF-MRAS. The performance of the drive is tested under different operating conditions, such as no-load forward motoring and reverse motoring mode with load acceptance and rejection capability. Furthermore, a sudden change in the speed or load is considered.

The speed performance of the IM drive at no load is shown in Fig. 7 with different adaption schemes. Conventional RF-MRAS has a steady-state error (SSE) during the starting of the IM drive, as shown in Fig. 7a. The SSE at the is due to the parameter mismatch of drive and the integrator's DC drift problem which causes inaccurate speed estimation in the reference and adaptation models. Fig. 7b illustrates the drive speed performance. A closer view of the drive speed tracking performance with the conventional RF-MRAS, modified RF-MRAS, and ANFIS-based RF-MRAS reveals that the performance of the drive has a good steady-state speed tracking over other adaption schemes when the reference speed is 100 r/min from 0 to 10 s. The steady-state error in the conventional adaption scheme is more because the non-linearity of the inverter is not fully eliminated. The ANFIS-based adaption scheme has a faster settling time with lesser oscillation and peak overshoot.

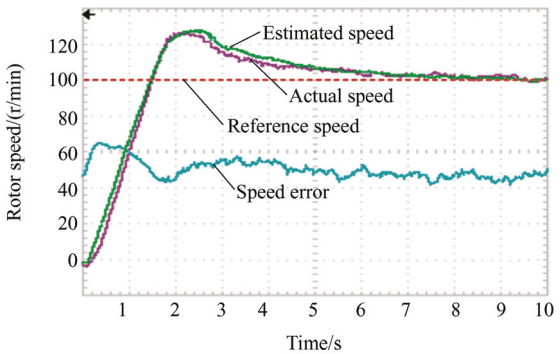

(a) Conventional RF-MRAS

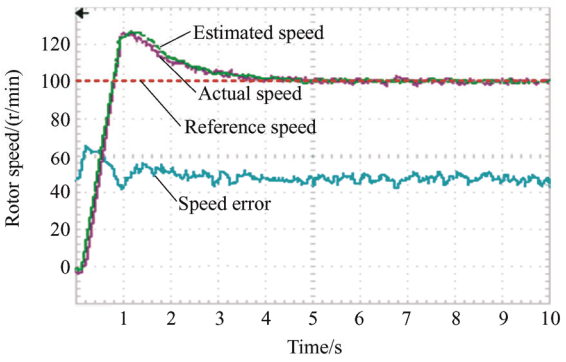

(b) Modified RF-MRAS using PI controller

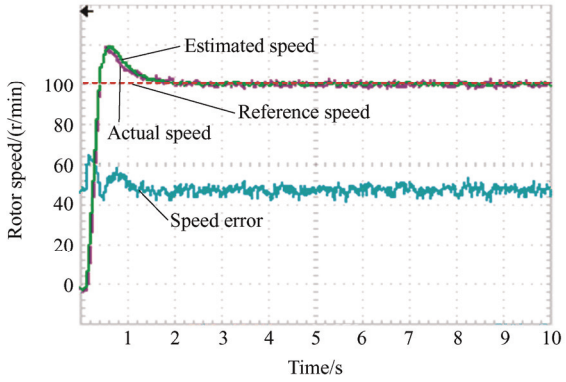

(c) Modified RF-MRAS using an ANFIS controller

Fig. 7 No-load drive performance when the reference speed is 100 r/min

The drive wide-range speed performance during sudden-change in speed from 100 r/min to 20 r/min with a step size of 20 r/min at t=12 s is presented in Fig. 8. The conventional and modified RF-MRAS have more oscillations during low-speed operation, whereas the wide speed response of the ANFIS-based adaption scheme has a good dynamic and steady-state performance. The drive load rejection capability is examined by applying 50% load torque at 12.5 s, and the load rejection capability of conventional and modified RF-MRAS is poor. However, the ANFIS-based method has good load torque performance even in the low-speed region. The performance of the ANFIS controller is better than that of the conventional and modified RF-MRAS schemes because of the decoupling of the rotor flux angle and slip in the sensorless vector control.

Some industrial applications require frequent reverse motoring operations. To verify this mode of operation, reverse motoring of the drive is conducted, and Fig. 9 illustrates the speed tracking performance over a wide range of speed. When a step changes in reference speed, the forward motoring mode reverses the motoring mode at 23 s. The conventional and modified RF-MRAS speed response is better at 100 r/min; however, during zero speed operation, the drive response does not follow the reference speed and it oscillates, whereas in the ANFIS scheme, the drive follows the reference speed even in zero-speed operation and does not oscillate. This is because of the addition of compensating voltage and using ANFIS in the adaption scheme; thus, the rotor flux component of the voltage and the current model are equal and makes the estimation speed equal to the reference speed.

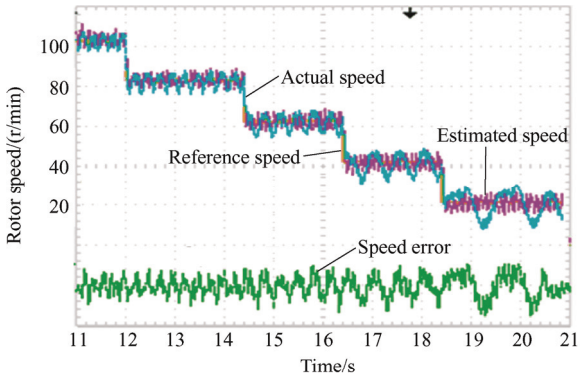

(a) Conventional RF-MRAS

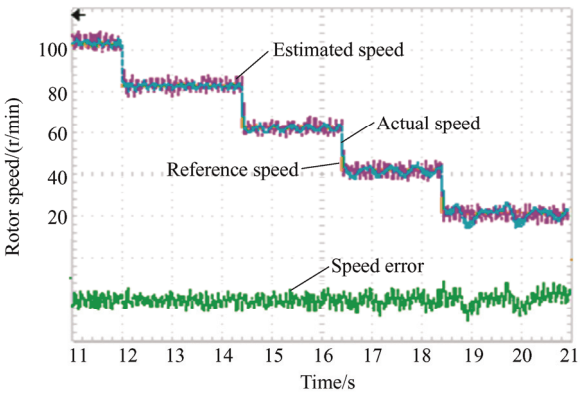

(b) Modified RF-MRAS with a PI controller

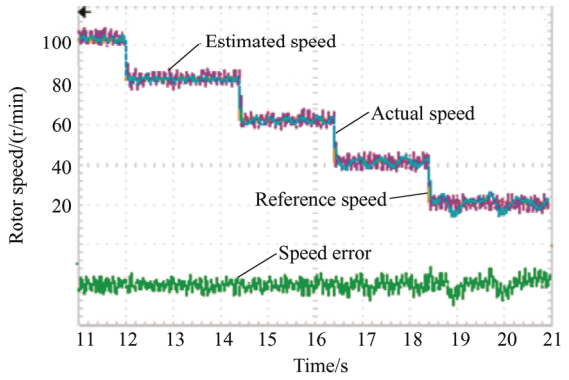

(c) Modified RF-MRAS with ANFIS controller

Fig. 8 (Top to bottom) speed tracking performance of the IM drive subjected to 50% of the rated load applied at 11.5 s

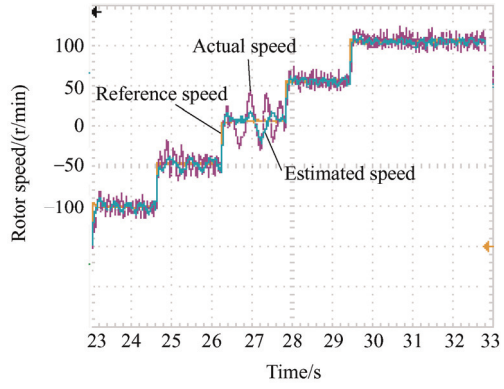

(a) Conventional RF-MRAS

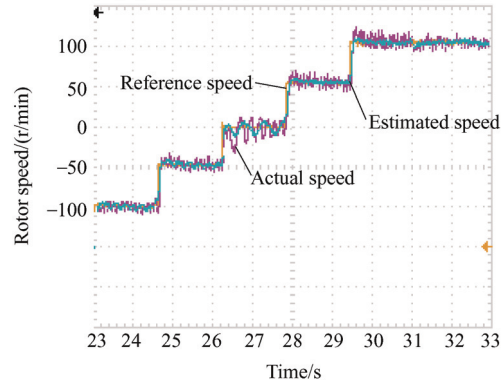

(b) Modified RF-MRAS with a PI controller

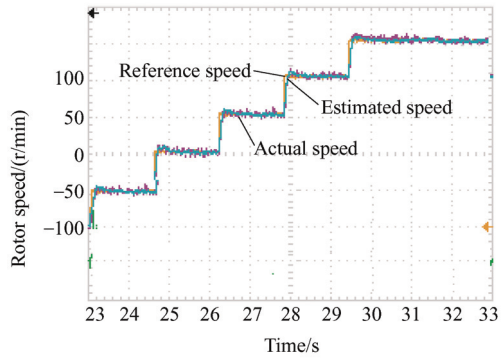

(c) Modified RF-MRAS with an ANFIS controller

Fig. 9 Performance of the IM drive from reverse motoring mode to forward motoring mode

The zoomed view of the speed tracing performance of the drives, illustrated in Fig. 10, from t=30 s shows the load acceptance performance with 50% of the rated load capacity. Fig. 10 shows the performance of the conventional RF-MRAS, modified voltage model, and ANFIS-based scheme. The experimental result of the drive suggests that the ANFIS-based scheme performs better than conventional and modified RF-MRAS when the load is applied at t=30.5 s; the actual rotor speed has a higher peak overshoot and oscillatory around the reference speed. The ANFIS-based control scheme has smoother torque and speed response, which is illustrated in a zoomed view of the speed tracking response with load torque applied to the speed observer, as shown in Fig. 10.

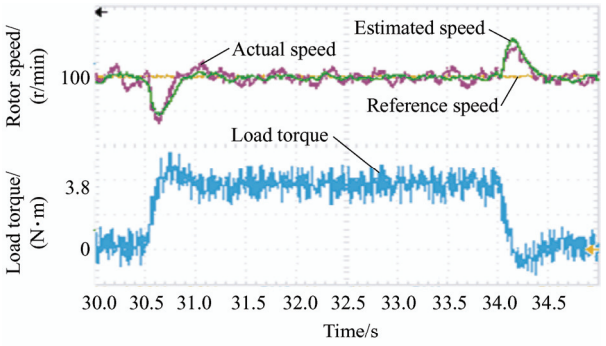

(a) Conventional RF-MRAS

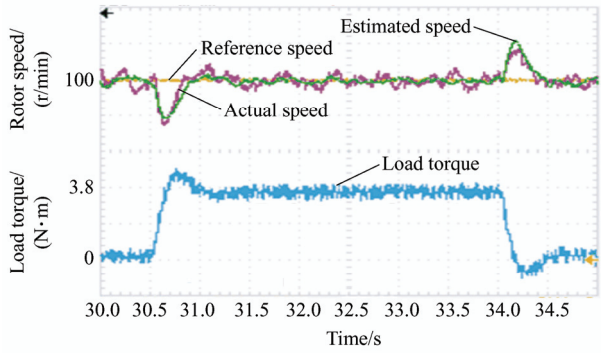

(b) Modified RF-MRAS with a PI controller

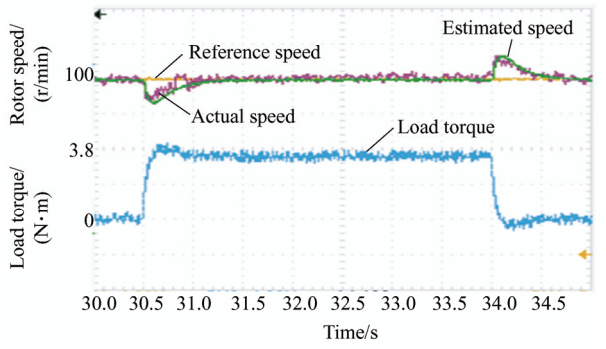

(c) Modified RF-MRAS with an ANFIS controller

Fig. 10 (Top to Bottom) zoomed view speed response at 100 r/min with different load torques

The three-level inverter voltages at steady state for conventional RF-MRAS, modified RF-MRAS with PI controller, and modified RF-MRAS with ANFIS controller are presented in Fig. 11. In Fig. 11a, the stator voltage response of conventional RFMRAS has the highest ripple content compared to the other methods. The variation of the stator current during low-speed operation for conventional RF-MRAS, modified RF-MRAS and ANFIS-based RFMARS is illustrated in Fig. 12. In Fig. 12c, the stator current response ANFIS-based RFMRAS is smoother compared to other methods and its harmonic content is lower.

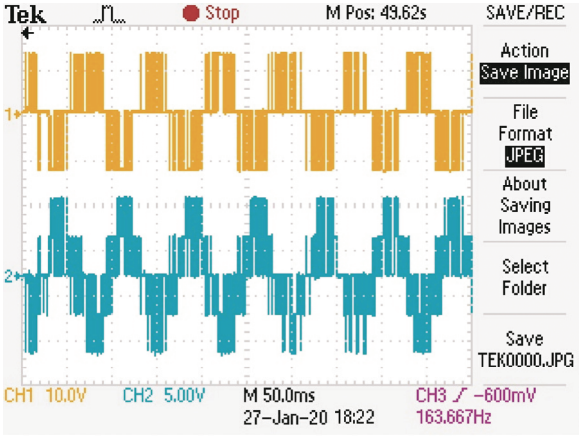

(a) Conventional RF-MRAS

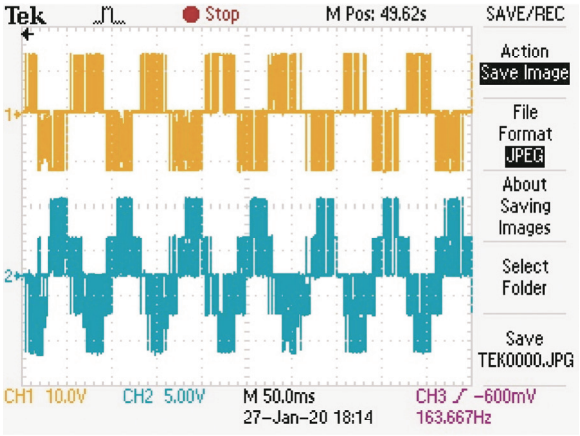

(b) Modified RF-MRAS with a PI controller

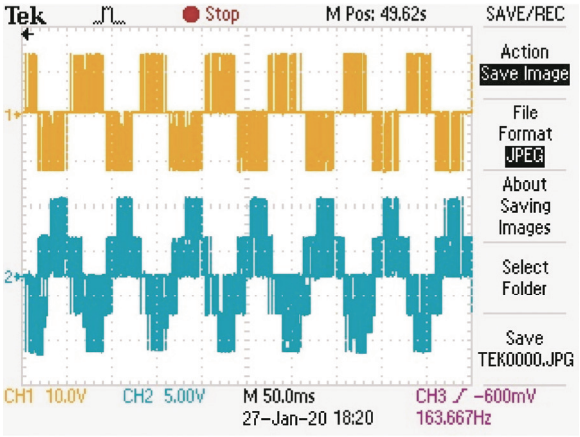

(c) Modified RF-MRAS with an ANFIS controller

Fig. 11 Inverter voltages at steady state of two and three-level inverter

Tab. 2 illustrates the performance of the IM drive with different adaptive mechanisms. The % percentage overshoot and settling time is taken as reference for comparative analysis of performance in conventional RF-MRAS, conventional RF-MRAS with modified voltage model and ANFIS with modified RF-MRAS when the drive is subjected to different operating conditions.

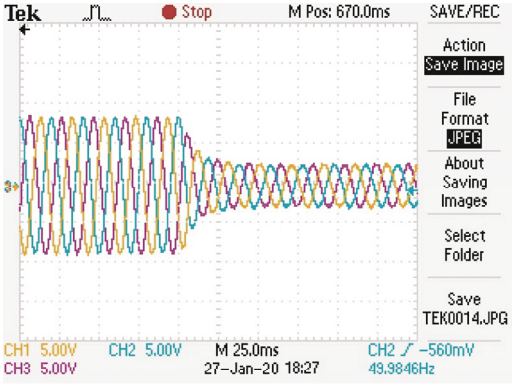

(a) Conventional RF-MRAS

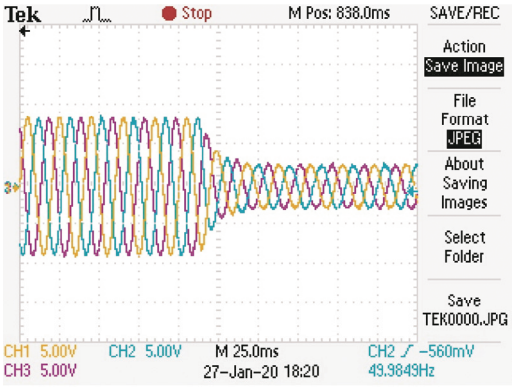

(b) Modified RF-MRAS with a PI controller

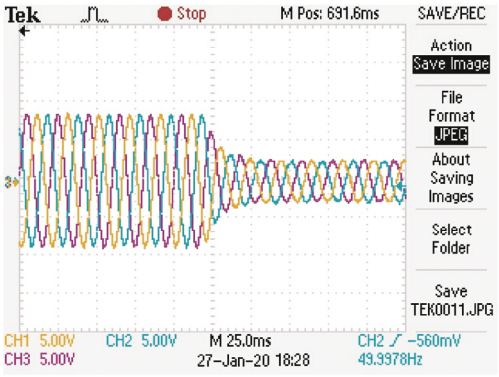

(c) Modified RF-MRAS with an ANFIS controller

Fig. 12 Stator current variation of three-level inverter during speed change state

The performance of the modified RF-MRAS is resonable compared to that of conventional RF-MRAS. In the beginning, the SSE in the conventional RF-MRAS with 40% overshoot in the speed response and 4 s settling time is improved by modified RF-MRAS and modified RF-MRAS using ANFIS to 15% and 1.3 s only. This shows a smooth change in the speed response.

The load rejection capability was tested by applying a 50% load torque at t=11.5 s, and the conventional RF-MRAS has 14% overshoot with a 1.5 s settling time. The overshoot and settling time

are reduced in the modified RF-MRAS with ANFIS because the rotor field angle is the same as the reference field angle. However, in the conventional RF-MRAS, the SSE presented owing to the stator resistance variation and MRAS scheme is dependent on the machine parameter. Further, the drive reaches a steady state near t=28 s. The drive response when 65% load torque is applied at t=30.5 s is used to verify the variation in the load torque perturbation.

Tab. 2 Comparison of the percentage overshoot or undershoot (M_P) and settling time (T_s) in the different adaptive schemes in speed sensor less control of IM drive methods for estimating the rotor speed

Operating condition	Parameter	Conventional RF-MRAS	Modified RF-MRAS	Modified RF-MRAS using ANFIS
Starting of drive when reference speed (0-100 r/min)	M_P(%)	30	25	18
	T_s/s	8	4	2
Step change in reference speed (form 100 r/min to 80 r/min), without load	M_P(%)	14	11	8
	T_s/s	1.5	0.9	0.6
Load rejection capability, 50% of rated load torque	M_P(%)	22	14	9
	T_s/s	1.29	0.9	0.5
Sudden change in speed (from 80 r/min to 60 r/min)	M_P(%)	18	13	11
	T_s/s	1.6	1.3	0.95
Change in reference speed (from 60 r/min to 40 r/min)	M_P(%)	21	15	13
	T_s/s	2	1.8	1.3
Sudden change in reference speed (from 40 r/min to 20 r/min)	M_P(%)	25	18	15
	T_s/s	Unstable	3	1.5
In reverse motoring speed change reference(form 100 r/min to 50 r/min)	M_P(%)	7.4	4.5	3.0
	T_s/s	3.1	2.2	1.1
Reverse to forward motoring mode, speed form 50 r/min to 10 r/min	M_P(%)	4.5	4.0	2.5
	T_s/s	Unstable	Unstable	0.9
Sudden change in speed (form 10 r/min to 50 r/min)	M_P(%)	15	10	5
	T_s/s	2.2	1.1	0.5
Change in reference speed (form 50 r/min to 100 r/min)	M_P(%)	8.5	5.5	2.0
	T_s/s	1.1	0.9	0.35

5 Conclusions

The low-speed response of the IM drive using the sensorless vector control technique is improved by the modified RF-MRAS with different adaptation schemes, such as conventional PI and ANFIS controllers, and their results are compared. The problem of DC drift and inverter nonlinearity of the RF-MRAS-based technique is reduced by modifying the reference and adaptive models. The compensating voltage was added to the rotor flux component. The voltage model and current model flux components provide accurate speed estimation. The ANFIS controller provides immunity to the machine parameter variation. From the simulation, the training data for the ANFIS is considered. In low-speed operation, the ANFIS controller reduces the SSE in the closed-loop operation. The three-level NPC inverter provides a good quality output voltage and reduces the voltage stress across the switch. All the results are taken from the experimental setup of the 1HP IM drive in real-time using a dSPACE DS 1104 processor.

References

[1] I M Alsofyani, N R N Idris. A review on sensorless techniques for sustainable reliablity and efficient variable frequency drives of induction motors. *Renewable and Sustainable Energy Reviews*, 2013, 24: 111-121.

[2] M H V Reddy, K S Gowri, T B Reddy, et al. Effect of center voltage vectors (CVVs) of three-level space plane on the performance of dual inverter fed open end winding

induction motor drive. *Chinese Journal of Electrical Engineering*, 2019, 5(2): 43-55.

[3] D Jiang, P Ning, R Lai, et al. Modular design method for motor drives. *Chinese Journal of Electrical Engineering*, 2018, 4(1): 1-10.

[4] A Tripathi, G Narayanan. Torque ripple minimization in neutral-point-clamped three-level inverter fed induction motor drives operated at low-switching-frequency. *IEEE Transactions on Industry Applications*, 2018, 54(3): 2370-2380.

[5] M A Hannan, J A Ali, A Mohamed, et al. Optimization techniques to enhance the performance of induction motor drives: A review. *Renewable and Sustainable Energy Reviews*, 2018, 81(2): 1611-1626.

[6] D Giribabu, S P Srivastava, M K Pathak. Modified reference model for rotor flux-based MRAS speed observer using neural network controller. *IETE Journal of Research 2019*, 65(1): 80-95.

[7] C Liu, Y Luo. Overview of advanced control strategies for electric machines. *Chinese Journal of Electrical Engineering*, 2017, 3(2): 53-61.

[8] D S Zinger, F Profumo, T A Lipo, et al. A direct field-oriented controller for induction motor drives using tapped stator windings. *IEEE Transactions on Power Electronics*, 1990, 5(4): 446-453.

[9] S K Kakodia, G Dyanamina. Field oriented control of three-level neutral point clamped inverter fed IM drive. *9th Annual Information Technology, Electromechanical Engineering and Microelectronics Conference,* 2019: 24-29.

[10] R Kumar, S Das, P Syam, et al. Review on model reference adaptive system for sensorless vector control of induction motor drives. *IET Electric Power Applications*, 2015, 9(7): 496-511.

[11] A Pal, S Das, A K Chattopadhyay. An improved rotor flux space vector based MRAS for field-oriented control of induction motor drives. *IEEE Transactions on Power Electronics*, 2018, 33(6): 5131-5141.

[12] M Ma, Z Wang, Q Yang, et al. Vector control strategy of a T-type three-level converter driving a switched reluctance motor. *Chinese Journal of Electrical Engineering*, 2019, 5(4): 15-21.

[13] I Takahashi, T Noguchi. A new quick-response and high-efficiency control strategy of an induction motor. *IEEE Transactions on Industry Applications*, 1986, IA-22(5): 820-827.

[14] D Casadei, F Profumo, G Serra, et al. FOC and DTC: Two viable schemes for induction motors torque control. *IEEE Transactions on Power Electronics*, 2002, 17(5): 779-787.

[15] Y Zhang, B Xia, H Yang, et al. Overview of model predictive control for induction motor drives. *Chinese Journal of Electrical Engineering*, 2016, 2(1): 62-76.

[16] M Habibullah, D D Lu, D Xiao, et al. Predictive torque control of induction motor sensorless drive fed by a 3L-NPC inverter. *IEEE Transactions on Industrial Informatics*, 2017, 13(1): 60-70.

[17] M H Vafaie, B M Dehkordi, P Moallem, et al. A new predictive direct torque control method for improving both steady-state and transient-state operations of the PMSM. *IEEE Transactions on Power Electronics*, 2016, 31(5): 3738-3753.

[18] Y Yoon, S Sul. Sensorless control for induction machines based on square-wave voltage injection. *IEEE Transactions on Power Electronics*, 2014, 29(7): 3637-3645.

[19] A Consoli, G Scarcella, A Testa. A new zero-frequency flux-position detection approach for direct-field-oriented-control drives. *IEEE Transactions on Industry Applications*, 2000, 36(3): 797-804.

[20] A V R Teja, C Chakraborty, S Maiti, et al. A new model reference adaptive controller for four quadrant vector controlled induction motor drives. *IEEE Transactions on Industrial Electronics*, 2012, 59(10): 3757-3767.

[21] D Giribabu, S P Srivastava, M K Pathak. Rotor flux based MRAS for sensorless operation of three level inverter fed induction motor. *2012 IEEE Students' Conference on Electrical, Electronics and Computer Science*, 2012: 1-4.

[22] T Orlowska-Kowalska, M Dybkowski. Stator-current-based MRAS estimator for a wide range speed-sensorless induction-motor drive. *IEEE Transactions on Industrial Electronics*, 2010, 57(4): 1296-1308.

[23] A V R Teja, V Verma, C Chakraborty. A new formulation of reactive-power-based model reference adaptive system for sensorless induction motor drive. *IEEE Transactions on Industrial Electronics*, 2015, 62(11): 6797-6808.

[24] R J Kerkman, T M Rowan, D Leggate. Indirect field-oriented control of an induction motor in the field-weakening region. *IEEE Transactions on Industry Applications*, 1992, 28(4): 850-857.

[25] D P Marčetić, I R Krčmar, M A Gecić, et al. Discrete rotor flux and speed estimators for high-speed shaft-sensorless IM drives. *IEEE Transactions on Industrial Electronics*, 2014, 61(6): 3099-3108.

[26] B Karanayil, M F Rahman, C Grantham. An implementation of a programmable cascaded low-pass filter for a rotor flux synthesizer for an induction motor drive. *IEEE Transactions on Power Electronics*, 2004, 19(2): 257-263.

[27] R Raute, C Caruana, C S Staines, et al. Sensorless control of induction machines at low and zero speed by using PWM harmonics for rotor-bar slotting detection. *IEEE Transactions on Industry Applications*, 2010, 46(5): 1989-1998.

[28] R Raute, C Caruana, C S Staines, et al. Staines analysis and compensation of inverter nonlinearity effect on a sensorless PMSM drive at very low and zero speed operation. *IEEE Transactions on Industrial Electronics*, 2010, 57(12): 4065-4074.

[29] D Giribabu, R H Vardhan, R Prasad. Multi level inverter fed indirect vector control of induction motor using type 2 fuzzy logic controller. *2016 International Conference on Electrical, Electronics, and Optimization Techniques (ICEEOT)*, 2016: 2605-2610.

[30] S Shukla, B Singh. Adaptive speed estimation with fuzzy logic control for PV-grid interactive induction motor drive-based water pumping. *IET Power Electronics*, 2019, 12: 1554-1562.

[31] S K Kakodia, G Dyanamina. Indirect vector control of IM drive fed with three level DCI. *2019 IEEE International Conference on Electrical, Computer and Communication Technologies (ICECCT)*, 2019: 1-6.

[32] S M Gadoue, D Giaouris, J W Finch. MRAS sensorless vector control of an induction motor using new sliding-mode and fuzzy-logic adaptation mechanisms. *IEEE Trans. Energy Convers*., 2010, 25(2): 394-402.

[33] S Maiti, V Verma, C Chakraborty, et al. An adaptive speed sensorless induction motor drive with artificial neural network for stability enhancement. *IEEE Transactions on Industrial Informatics*, 2012, 8: 757-766.

[34] G Dyanamina, M K Pathak, S P Srivastava. Parallel stator resistance estimator using neural networks for rotor flux based model reference adaptive system speed observer. *Electric Power Components and Systems*, 2016, 44: 658-672.

[35] W Ding, D Liang. Modeling of a 6/4 switched reluctance motor using adaptive neural fuzzy inference system. *IEEE Transactions on Magnetics*, 2008, 44(7): 1796-1804.

Giribabu Dyanamina received a B.Tech. degree in electrical and electronics engineering from Jawaharlal Nehru Technological University (JNTU), Hyderabad, Telangana, India in 2006, and his M.T. degree in power electronics from JNTU in 2008, and Ph.D. degree in electrical engineering in the Indian Institute of Technology Roorkee (IITR), Uttarakhand, India. In 2013, he joined the National Institute of Technology Kurukshetra (NIT-KKR), Haryana, India, as an assistant professor in the Electrical Engineering Department. In 2019, he joined the Maulana Azad National Institute of Technology Bhopal (MANIT-B), India, the Electrical Engineering Department, where he works as an assistant professor. He is a senior IEEE member. His research interests include sensorless speed control of electric drives, multi-level inverters, AI, and renewable energy sources.

Sanjay Kumar Kakodia received a B.Tech. degree in electrical engineering from Rajasthan Technical University (RTU) Kota, Rajasthan, India, in 2016. He received his M.Tech. degree in power electronics and drives from the National Institute of Technology, Kurukshetra (NIT-KKR), India in 2019. He was worked as an assistant professor in MITRC Alwar, Rajasthan, India. He is currently research scholar in the Electrical Engineering Department, Maulana Azad National Institute of Technology Bhopal (MANIT-B), India. His research interests include sensorless speed control of IM drives and multilevel inverters.